

Available online at [www.sciencedirect.com](http://www.sciencedirect.com)

ScienceDirect

journal homepage: <http://www.elsevier.com/locate/acme>

## Original Research Article

# Acoustic emission monitoring of granite under bending and shear loading

A.C. Mpalaskas<sup>a</sup>, T.E. Matikas<sup>a</sup>, D. Van Hemelrijck<sup>b</sup>,  
G.S. Papakitsos<sup>a</sup>, D.G. Aggelis<sup>b,\*</sup>

<sup>a</sup> Department of Materials Science and Engineering, University of Ioannina, Greece

<sup>b</sup> Department of Mechanics of Materials and Constructions, Vrije Universiteit Brussel, Belgium

## ARTICLE INFO

## Article history:

Received 14 March 2015

Accepted 24 January 2016

Available online 27 February 2016

## Keywords:

Bending

Shear

Granite

Acoustic signature

Rise time

## ABSTRACT

In this study bending and shear fracture experiments on healthy and adhesively repaired granite samples with concurrent acoustic emission (AE) monitoring are discussed. AE can characterize the difference between the fracture modes using simple features analysis based on the activity of the early loading. It is the first time that such a direct correspondence between the stress field and the results of a monitoring technique emerge for granite. This offers new insight in the material's behavior especially in relation to complicated geometries where the dominant stress mode is not known a priori.

© 2016 Politechnika Wroclawska. Published by Elsevier Sp. z o.o. All rights reserved.

## 1. Introduction

Fracture of structural materials exhibits a typical succession. Micro-cracking due to tension occurs with low to moderate load and later shear phenomena tend to dominate [1]. Defining of the main fracture mode provides information on the fracture process and the structural behavior of the materials and structures. A suitable way to monitor fracture is the acoustic emission (AE) technique. AE utilizes piezoelectric sensors attached on the surface of the material to record the stress waves triggered after crack nucleation and propagation events in analogy to the earthquake activity but in smaller scale [2–4]. Several studies have been published on monitoring of fracture evolution [5–8], monitoring of corrosion [9], healing

[10] and creep in granite or other materials [11,12]. AE signals from cracking and debonding have been separated in composite structures, where in addition to the cracking of the matrix material, reinforcement in the form of bars, fibers or patches was detached from the matrix [13–15]. Recently shear and tensile patterns of fracture in the matrix material itself have been targeted in mortar, concrete and marble specimens [16–18]. This paper presents the AE activity during bending and shear tests of granite beams in laboratory. Mechanical behavior of granite is of interest in different fields, from restoration of cultural heritage monuments to underground engineering and excavation works [19–21]. AE has been used for monitoring the fracture and localizing the sources [20,21] while ultrasonics for correlations to the damage degree of granite materials [22]. AE total activity, event location and

\* Corresponding author. Tel.: +32 2 629 3541; fax: +32 2 6292928.

E-mail address: [daggelis@vub.ac.be](mailto:daggelis@vub.ac.be) (D.G. Aggelis).

<http://dx.doi.org/10.1016/j.acme.2016.01.006>

1644-9665/© 2016 Politechnika Wroclawska. Published by Elsevier Sp. z o.o. All rights reserved.

indices like the “b-value” have proven helpful to improve the difficulties in determining the damage level and the crack density of granite [23]. After the test, the specimens were repaired by epoxy resin with polyamide hardener, and loaded to failure a second time under the same mode in order to evaluate the degree of restoration of properties. This supplied information on the restoration power of adhesive repair for different loading patterns which is particularly important in cultural heritage engineering. AE was monitored by two resonant sensors enabling event location and allowing to capture all relevant activity due to material fracture excluding noise. The AE characteristics most sensitive to the changes in the stress field are presented and discussed.

## 2. Experimental details

### 2.1. Materials-repair method

Two types of granite were used, one named Giallo Rusty from China with a density of  $2470 \text{ kg/m}^3$  and the other named Tropical Black with a density of  $2613 \text{ kg/m}^3$  from Italy. For convenience the first type will be addressed as G2 and the next as G6. The specimens were prismatic of size  $40 \text{ mm} \times 30 \text{ mm} \times 160 \text{ mm}$ . Three of the specimens per granite type were subjected to three-point bending according to EN 13892-2:2002 see (Fig. 1a). The load was applied at a constant rate of  $50 \text{ N/s}$  and the loading was automatically terminated at the moment of load drop. The setup was modified for the test of the other three specimens per granite type that were intended for the “shear” mode: a metal tab of length of  $50 \text{ mm}$  was placed in the center above the specimen (Fig. 1b). Although at the three-point bending test, the crack starts from the central point of the bottom side due to the tensile stresses, for the modified test, the metal tabs used for support reduce the free bottom span and leave only a small zone available for shearing which is triggered by notches on both top and bottom sides of the specimen of  $5 \text{ mm}$  depth (right in Fig. 1b). In a previous study, static FEM simulations confirmed that shear stresses obtain much higher values than normal at the notch tip [17]. Additionally, Fig. 1a and b shows typical granite specimens during the bending and shear test respectively.

After bending and shear fracture has occurred all the specimens were repaired in the crack surface with a two-component bonding system based on epoxy resin and hardener named “Epoxyol” in its commercial product name. It is a specially formulated, high viscosity, two component polyester marble adhesive-putty used to bond and fill for repair purposes with hardening time of approximately  $5\text{--}6 \text{ h}$  [24]. The bonding was carefully established so that the original geometry of the specimen was not altered.

### 2.2. AE testing

AE monitoring took place by means of two piezoelectric sensors (R15, Mistras). Their resonance comes at  $150 \text{ kHz}$  and their positions on the specimens are shown in Fig. 1. One sensor was placed  $15 \text{ mm}$  away from the expected crack, which was secured by a notch. The second sensor was placed

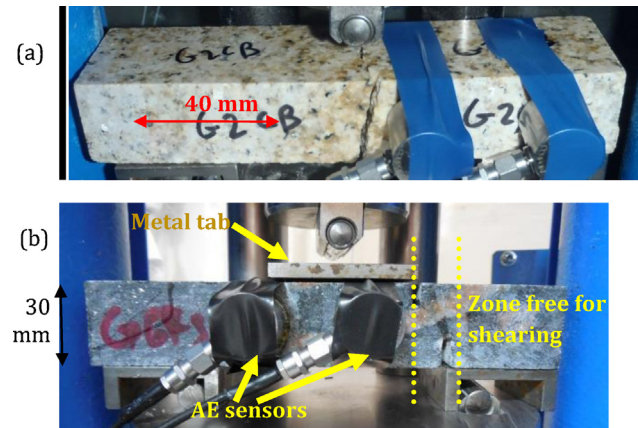


Fig. 1 – (a) Three point bending and (b) shear test of granite with concurrent AE monitoring by two sensors.

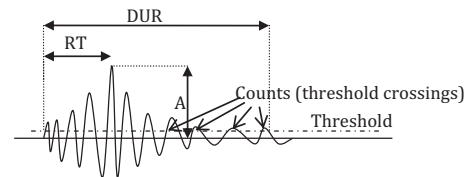
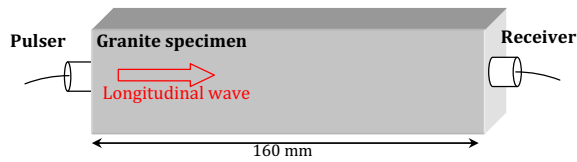


Fig. 2 – Typical AE waveform and its basic characteristics.

$40 \text{ mm}$  away. Both sensors were positioned at the same side of the crack in order to be able to characterize the distortion of the signals as they propagate for the additional distance of  $40 \text{ mm}$ . Acoustic coupling was improved by silicon grease between the sensors face and the specimens' surface. AE activity was captured by a two-channel PCI-2 Mistras board with sampling rate of  $5 \text{ MHz}$ . The threshold was  $40 \text{ dB}$ , as well as the pre-amplification. A schematic representation of a waveform is seen in Fig. 2. Some of the main features are the maximum amplitude,  $A$  (usually in  $\text{dB}$ ), and the duration (period between the first and the last threshold crossing). The “rise time”,  $RT$  (which is the time between the first threshold crossing and the point of peak amplitude in  $\mu\text{s}$ ) is related to the fracture mode of the crack. It has been shown that shear type of failure like debonding of patches, pull-out of fibers and shear matrix cracking induces signals with longer duration and  $RT$ , mainly attributed to the higher proportion of transverse elastic waves that are triggered by the parallel motion of the crack tips [13,14,16–18]. Frequency content can be measured by  $AF$  (average frequency), which is the total number of threshold crossings divided by the duration while there are other indices based on the spectrum of the FFT.

Before the fracture tests, ultrasonic measurements were conducted on the samples, according to Fig. 3. They were conducted by the same piezoelectric transducers as the AE monitoring. The electric excitation triggering the pulser was one cycle of  $150 \text{ kHz}$ . The received signal was digitized with  $10 \text{ MHz}$  sampling and the first detectable disturbance of the waveform was picked manually. The measurement corresponds to the longitudinal waves which are the fastest type.



**Fig. 3 – Schematic representation of ultrasonic test with longitudinal waves.**

Pulse velocity was calculated by the length of the specimens (160 mm) over the wave transit time.

Type	Specimen	Pulse velocity (m/s)	Elastic modulus <sup>a</sup> (GPa)
Giallo Rusty	G2AB	4969	61.0
	G2BB	5333	70.3
	G2CB	5031	62.6
Tropical Black	G6AB	5735	85.9
	G6BB	6084	96.7
	G6CB	6061	96.0

<sup>a</sup> Elastic modulus E, was calculated through relation  $E = \rho C^2$ , where  $\rho$  is density and C the pulse velocity.

### 3. Results

#### 3.1. Ultrasonic and mechanical results

Table 1 includes the results of the ultrasonic pulse velocity test. Specimens of type G6 exhibited values close or above 6000 m/s, while G2 lower, around 5000 m/s. This implies higher stiffness for G6. Indeed based on the densities of the materials and the measured wave velocities, the elastic moduli values are between 60 and 70 GPa for type G2 and around 90 GPa for type G6, as seen in Table 1. The maximum loads for both bending and shear tests for the intact and the repaired version of the specimens are included in Table 2. The intact Tropical Black (G6) specimens exhibited steadily higher bending load which is in accordance with its higher ultrasonic pulse velocity. In the shear test, there is again a difference in favor of G6 in average (approximately 1 kN), but with overlap between the populations. Concerning reloading after repair, all specimens maintained their initial fracture surface and for the bending test there is a noticeable restoration of approximately 50–75% of the initial strength. For the shear, the restoration is much lower between 30 and 40%. This is for both types of granite indicating that after repair by epoxy, the material is more susceptible to shear, while for bending the order of load that can be carried is quite restored to the “virgin” state, though not completely. Photographs of typical specimens after fracture are seen in Fig. 4.

#### 3.2. Acoustic emission activity – bending test

Before presenting the differences of AE descriptors based on the mode of test, the curves of the cumulative AE events activity vs. time can be seen in Fig. 5. These curves reveal the rate of nucleation/propagation of cracks and help to assess the time or load during which most of the damage is occurring. The left column concerns bending of three healthy specimens and right concerns the reloading of the same specimens after repair by epoxy. The depicted activity concerns the “events” and not the whole number of recorded AE hits. Specifically, by applying two sensors, it was possible to activate “linear localization”. Practically, by the time delay between acquisitions of two successive signals by the two sensors, the actual location of the source can be calculated. Localization makes use of the ultrasonic pulse velocity that was measured beforehand. This way, the activity concentrated in a zone of 10 mm around the crack was isolated in the specific analysis. This serves two purposes; one is to eliminate possible sources of noise that may contribute to the overall recorded activity but they are not actually due to the fracture in the intended mode and location. The second is to avoid contributions by the attenuation and dispersion of the material: isolating the origin of the events in a narrow zone of 10 mm, it is sure that the path of propagation was very similar for all the different events until being recorded by the sensor. Therefore, possible influence by attenuation and material heterogeneity is kept to a minimum. The information presented in this analysis comes from the sensor closer to the crack in order, as

Type	Specimen	Bending (kN)		Strength restoration (%)	Specimen	Shear (kN)		Strength restoration (%)
		Healthy	Repaired			Healthy	Repaired	
Giallo Rusty	G2AB	3.626	2.303	63.5	G2DS	5.491	1.513	27.6
	G2BB	3.883	1.882	48.5	G2ES	3.626	1.395	38.5
	G2CB	3.836	2.759	71.9	G2FS	4.074	1.138	27.9
Tropical Black	G6AB	5.286	3.527	61.8	G6DS	4.222	1.576	37.3
	G6BB	4.89	2.989	51.1	G6ES	7.209	2.152	29.9
	G6CB	4.444	2.287	73.8	G6FS	4.771	1.693	35.5

Last letter “B” in the codenames denotes “bending” and “S” denotes “shear”.



Fig. 4 – Typical specimens after fracture (a) bending, (b) shear.

aforementioned, to clear the waveforms from effects of distortion from the additional propagation of 40 mm, even though the distance is quite short.

The plots start at time zero when the central loading point touched the specimen. This contact resulted in a small number of hits, but not in events as it did not originate from the fracture zone and it was not related to the fracture process. After a period (A) of silence indicating no cracking activity due to negligible stresses, a few events were recorded (point B). Another plateau followed (C) and at point D a moderate activity started to be noted, continuing throughout period E. Finally, there is an increase of AE rate (stage F) leading to the final fracture of the specimen. All healthy specimens seem to follow a more or less similar pattern of AE activity. The only remark is that stage “E” for the specimen G2CB exhibits much less activity than the other two specimens. These plateaus in the AE activity have been observed in compression experiments of granite as well [25], and more specifically, two zones of “avalanche-like” activity interrupted by a long period of acoustic silence. This is related to initial micro cracking which is restrained, while the material accumulates elastic energy before mechanisms of larger scale become active.

The behavior of the same specimens at reloading after repair does not seem as uniform and cannot be described with the same stages. This is not surprising as the homogeneity of the material has been irreversibly changed leading to stronger experimental scatter between different samples. Indicatively, the second specimen (G2BB repaired) did not even exhibit a plateau once the emissions started at 31 s, while the last specimen (G2CB repaired) exhibited a large plateau between 35 and 55 s. On the other hand, the first specimen (G2AB repaired) had a stage of moderate activity.

The behavior of specimens from granite type G6 is shown in Fig. 6.

For the specimens of this granite type the same succession of stages seems to hold (especially the two last healthy specimens). Concerning the repaired, again there is not a unique trend, as the first specimen exhibited a long silence plateau, the second an exponential increase of AE and the last, a stage of moderate activity instead of plateau or exponential increase. One detail that can be mentioned is that the initial

plateau was slightly longer for the repaired specimens than the healthy in both categories. For the repaired version of the specimens this silent period was between 30 and 40 s, while for the healthy it was equal or shorter than 25 s. This can be attributed to the elasticity of the epoxy resin which is one order of magnitude lower than elastic modulus of granite. Therefore, under a certain displacement rate, it can strain for longer period of time before emitting acoustic signals due to irreversible cracking.

### 3.3. Acoustic emission activity – shear test

The corresponding AE activity for specimens G2 tested in shear is shown in Fig. 7. The behavior of the intact specimens, is shown at the left. All specimens exhibited a continuous line once the activity starts, without plateaus like the corresponding bending tests. It seems that shear micro-cracking was continuous without periods of stress build-up as was the case for bending. For the repaired specimens at the right of Fig. 7, the whole duration was shorter since the specimens failed at much lower load. The initial period of silence remains of the same order followed by a more or less linear path until failure.

The AE behavior of granite G6 is shown in Fig. 8. The trends remain similar for the healthy specimens, with the AE activity building up in a more or less linear way until failure. In this case, the repaired specimens showed a more uniform behavior, including an initial plateau, an increase of the rate followed by a slight decrease before the rise of the slope up to failure. The linear development to failure was not followed by the repaired specimens.

### 3.4. AE waveform parameters analysis

Apart from the total activity, AE parameters shed light in the fracture process and specifically have been used to characterize the fracture mode [26–28]. Therefore, it is deemed very important to check the values of AE parameters as it has been shown that they are sensitive to the different type of loading and the resulting fracture pattern. Of particular importance in this study is the rise time, RT, as shown in Fig. 2, which showed the most drastic changes between the two fracture modes. In

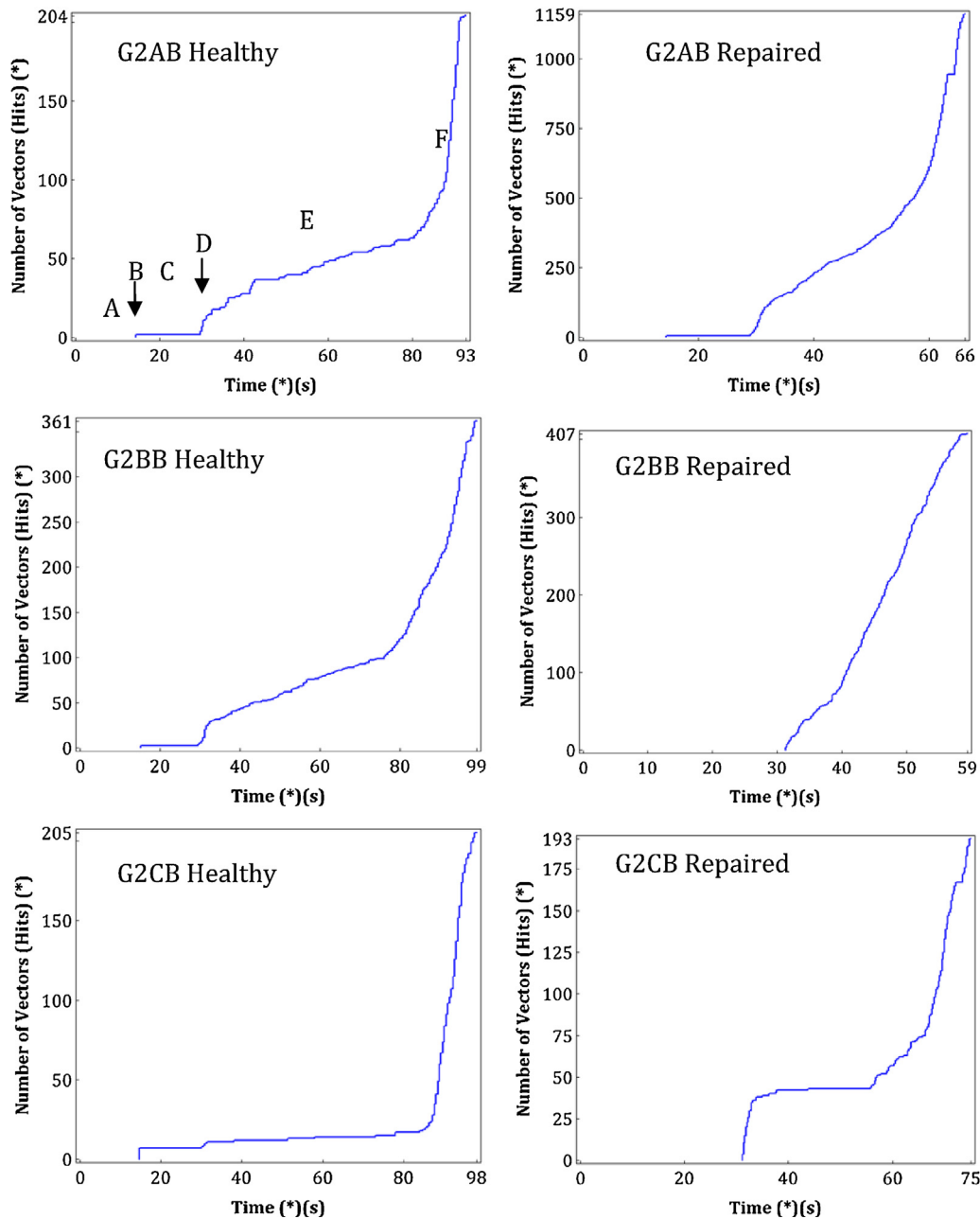


Fig. 5 – Accumulated AE activity of granite G2 vs. time for the bending test: left healthy, right repaired specimens.

order to analyze the development of the AE parameters during loading, indicative parts of the whole population were isolated as shown in Fig. 9. One part was taken during the early stage of the loading when the AE rate was still moderate (below 50% of ultimate, class 1, green) and the second just before final failure when the AE recording rate was much faster (class 2, blue).

The populations from all three specimens of each type were added together to produce a larger database of AE signals, received at initial loading stages (class 1) and before failure (class 2) separately for bending and shear loading. Fig. 10 shows the density distribution of the values of RT of the early class 1 for bending and shear of granite G2 (top) and G6 (bottom). Concerning bending of G2, most of the RT values are

below  $40 \mu\text{s}$  (see Fig. 10a), having a peak at  $20 \mu\text{s}$ . For the shear type of loading, the distribution moves to higher values up to  $100 \mu\text{s}$  (again Fig. 10a), while there is also a small peak at  $180 \mu\text{s}$ . The picture is quite similar for granite G6 in Fig. 10c; bending load results in RT mostly below  $40 \mu\text{s}$ , while the corresponding distribution for shear extends up to  $200 \mu\text{s}$ . This is a very direct indication of the influence of the stress tensor (normal-shear) to the AE exhibited during fracture and has never been measured in granite so far. In addition to the whole distributions as depicted in Fig. 10, the averages of the populations are very indicative; Bending of G2 and G6, results in average values of RT of  $45.1 \mu\text{s}$  and  $42.5 \mu\text{s}$  respectively, while for the shear tests the corresponding average RT values

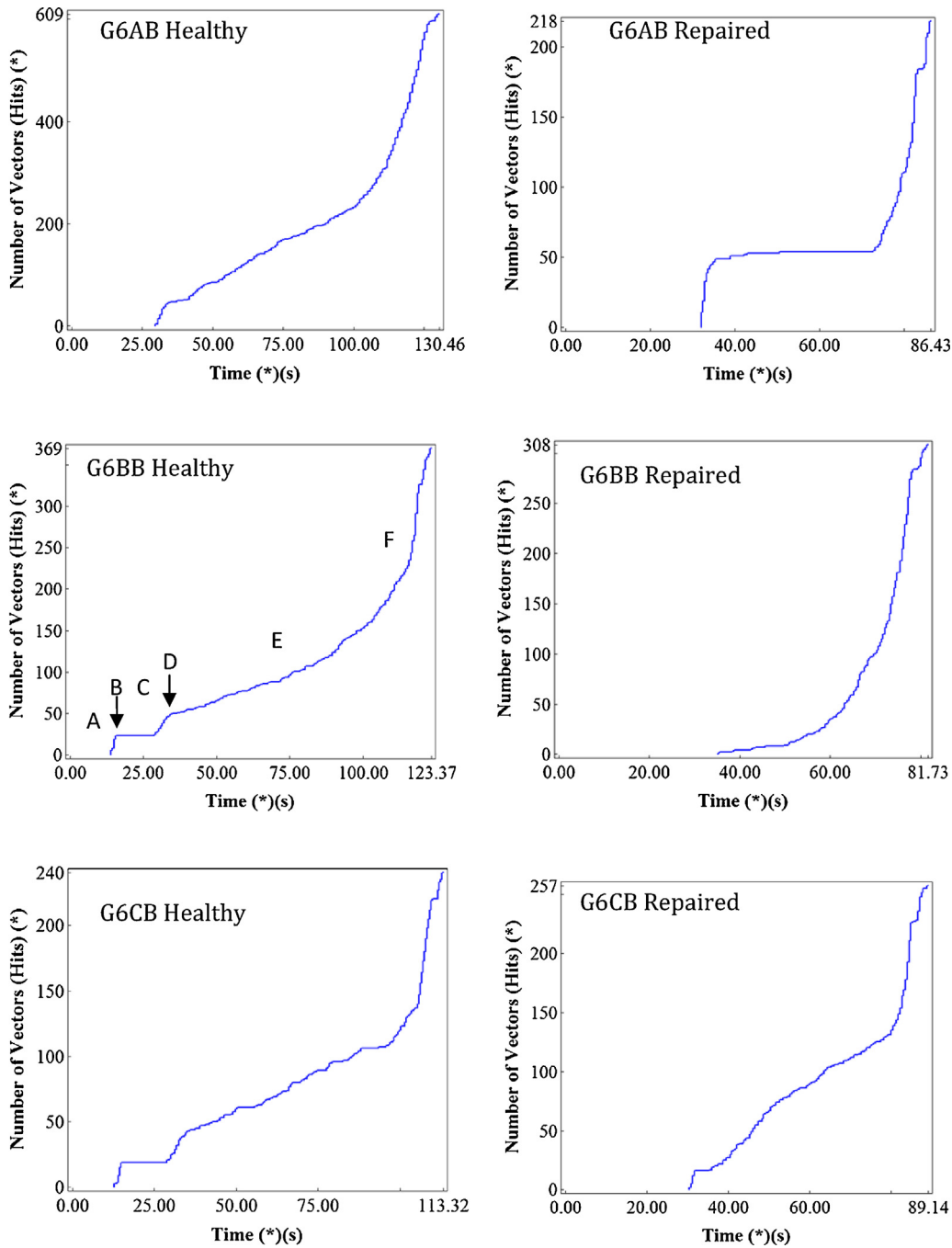


Fig. 6 – Accumulated AE activity of granite G6 vs. time for the bending test: left healthy, right repaired specimens.

are 210.8  $\mu$ s and 229.7  $\mu$ s, being four to five times higher. The reason can be related to the different wave modes (longitudinal or transverse) that are triggered by the motion of the crack sides under the dominant mode [30]. This enables the assessment of the type of stresses acting on the material by passive AE monitoring of the initial loading stage without inducing serious damage in the material (e.g. less than 50% of maximum load).

For the repaired version of the specimens things do not seem to change considerably (see Fig. 10b and d). For both material types, bending RTs are limited up to 40–60  $\mu$ s, while

shear ones extend to 200  $\mu$ s or more. In the case of Fig. 10d concerning granite G6, even though the highest peaks of RT distributions coincide at 20  $\mu$ s, the shear distribution extends to higher values and the average value is at 126  $\mu$ s compared to 57  $\mu$ s of bending. This shows that the intended fracture mode is followed even after repair confirming that AE is a suitable technique for passive characterization of the stress built-up and fracture accumulation. It should be mentioned that apart from the populations up to 300  $\mu$ s which are shown in the graphs, there are systematic differences in the higher regimes. Specifically, for the bending tests of both granites, only 2% of

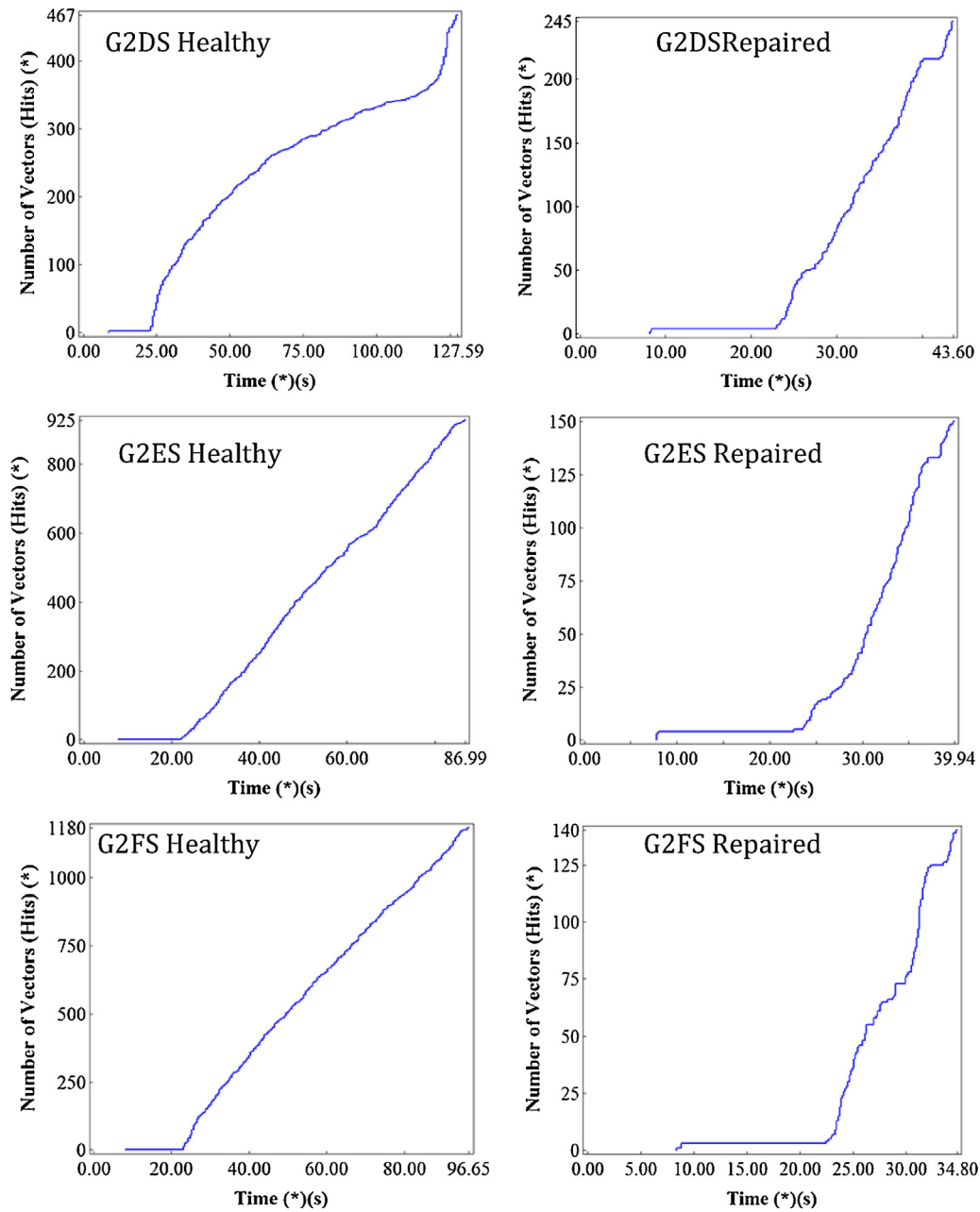


Fig. 7 – Accumulated AE activity of granite G2 vs. time for the shear test: left healthy, right repaired specimens.

the RT population is included above  $300 \mu\text{s}$ , while for shear this percentage is 10% leaving a substantial part of the population to higher values. This behavior of higher RT values corresponds to the different stress field, which as aforementioned targeted the shear type of failure and has been seen in materials like mortar and concrete [16,17]. Measuring the waveform parameters enables conclusions on the fracture mode simply using one sensor (essentially the 2nd is for noise removal in this case), while a more elaborate approach would be the moment tensor analysis (MTA) that requires multiple sensors. Though the results of MTA are quite detailed [31], application may not be practical in all situations since the number of at least six sensors is necessary for recording of each AE event.

It is interesting to note that these differences in the activity of class 1 were obtained much earlier than final fracture, before the load bearing capacity of the specimens has been compromised. Therefore, it is possible that after suitable study, a proof test with simultaneous recording by AE can reveal the dominant stress component as well as indicate the suitability of the repaired material to withstand the same loading pattern.

The behavior of the AE populations at higher load (class 2) is shown in Fig. 11. It is interesting to see that the differences between bending and shear in this case are much smaller. For granite G2, the density distribution of shear RT values has its peak at the same point (i.e. up to  $20 \mu\text{s}$ ) but is wider reaching to values up to  $200 \mu\text{s}$  (Fig. 11a). For G6 the distributions are

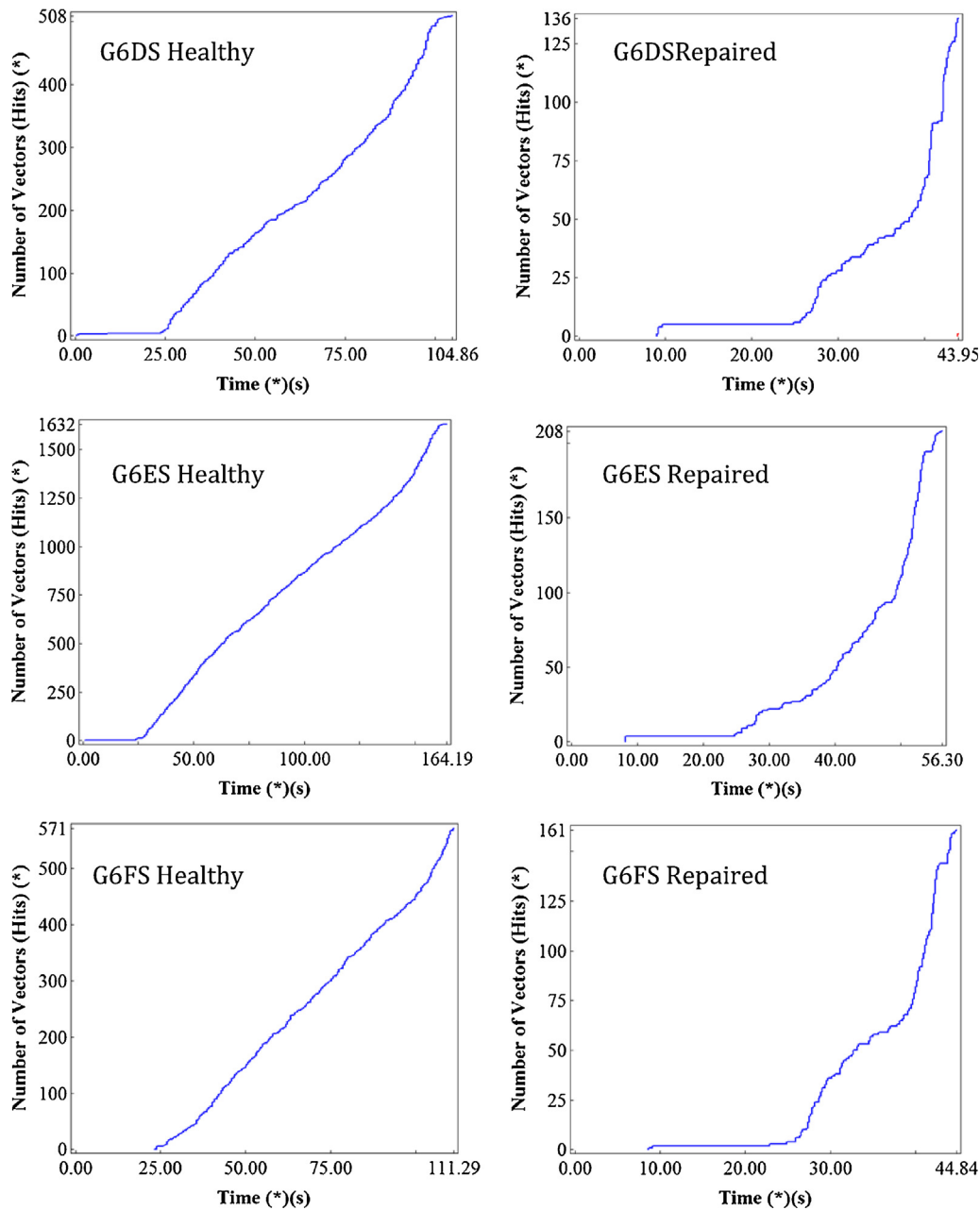


Fig. 8 – Accumulated AE activity of granite G6 vs. time for the shear test: left healthy, right repaired specimens.

essentially the same (Fig. 11c). This finding shows that after the initial micro-cracking is developed according to the different loading pattern (bending or “shear”), at the final stage of loading the material fractures nearly in the same way independent of the type of loading. This behavior, although should be further investigated, it has been evidenced in similar media where the regime near the load peak “is characterized by a strong strain localization, independent of the actual failure mechanism” and the energy dissipation is “a surface-dominated phenomenon, analogously to the tensile behavior” [5,32]. It is compatible with the assumption that the shear fracture occurs by the coalescence of tensile micro-cracks. Most of the systematic differences therefore, are seen in the early behavior, while later fracture (even from the “shear” test)

resembles tensile behavior, which justifies the low RT values during high load. It will be interesting to use FEM to simulate the stress field during fracture, in order to reveal how the dynamic stress tensor changes after the crack initiation, relatively to the initial stress field revealed by static simulations [17]. The repaired specimens' behavior is similar, with the “shear” distributions peaking at the same point but usually expanding to slightly higher values than “bending” (Fig. 11b and d). The above show that simple analysis can reveal the preliminary fracture mechanism and the tendencies that will be followed throughout loading. Experimental scatter is inherent with AE and therefore, it is almost impossible to completely separate the data hit by hit regarding their origin. However, taking into account an indicative group, the relative

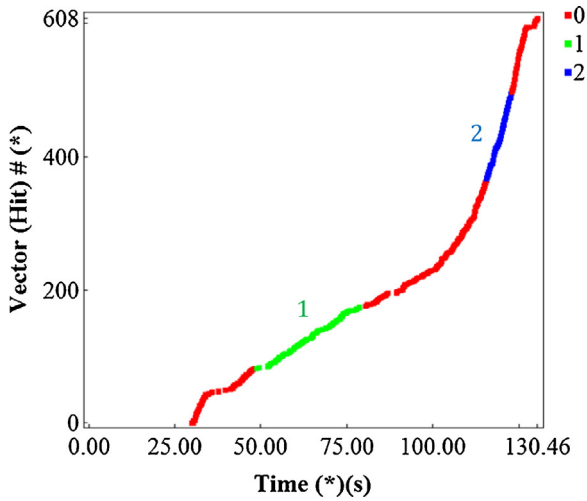


Fig. 9 – Cumulative history of events and indicative class separation using the Noesis software [29].

differences can be well identified and shed light in the damage process since, as shown the population distributions are quite different.

#### 4. Discussion

In this section some specific issues are discussed after the basic results were presented. The first point concerns the characterization of the fracture mode. This characterization is based, as aforementioned, on the initial static stress field as simulated by FEM analysis. For the so-called “shear” experiment, the ratio between shear and normal is more than 2 at the point of the notch [17]. Therefore, it is highlighted that although shear stress is high, this is not pure shear. We use the term “shear” for simplicity to denote mixed mode with stronger shear components. It is also highlighted that the microstructure of the material may well change the conditions of crack propagation from what is macroscopically calculated even in the static case, let alone the dynamic crack propagation. The present manuscript considers the initial “macroscopic” static loading conditions and not how the fracture process develops after crack initiation. From the moment the

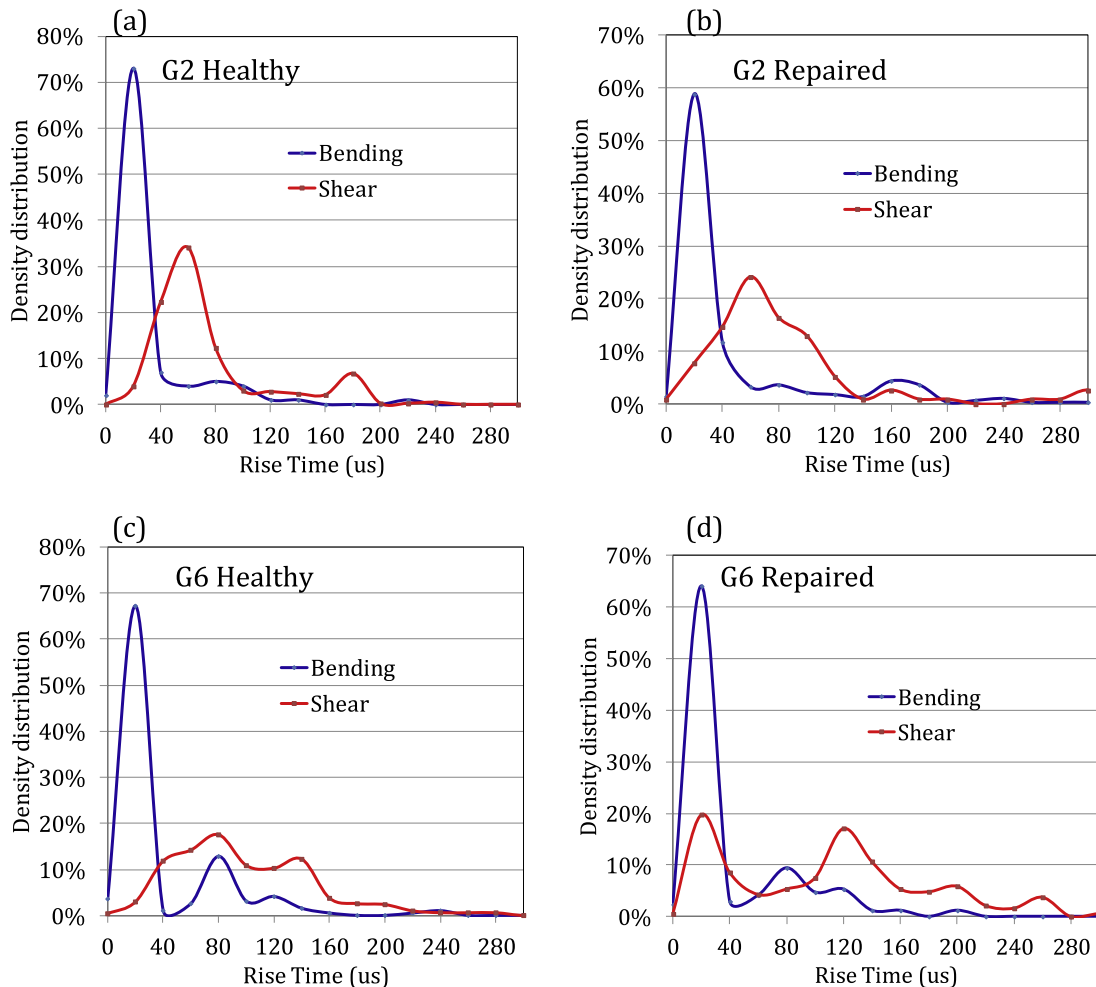
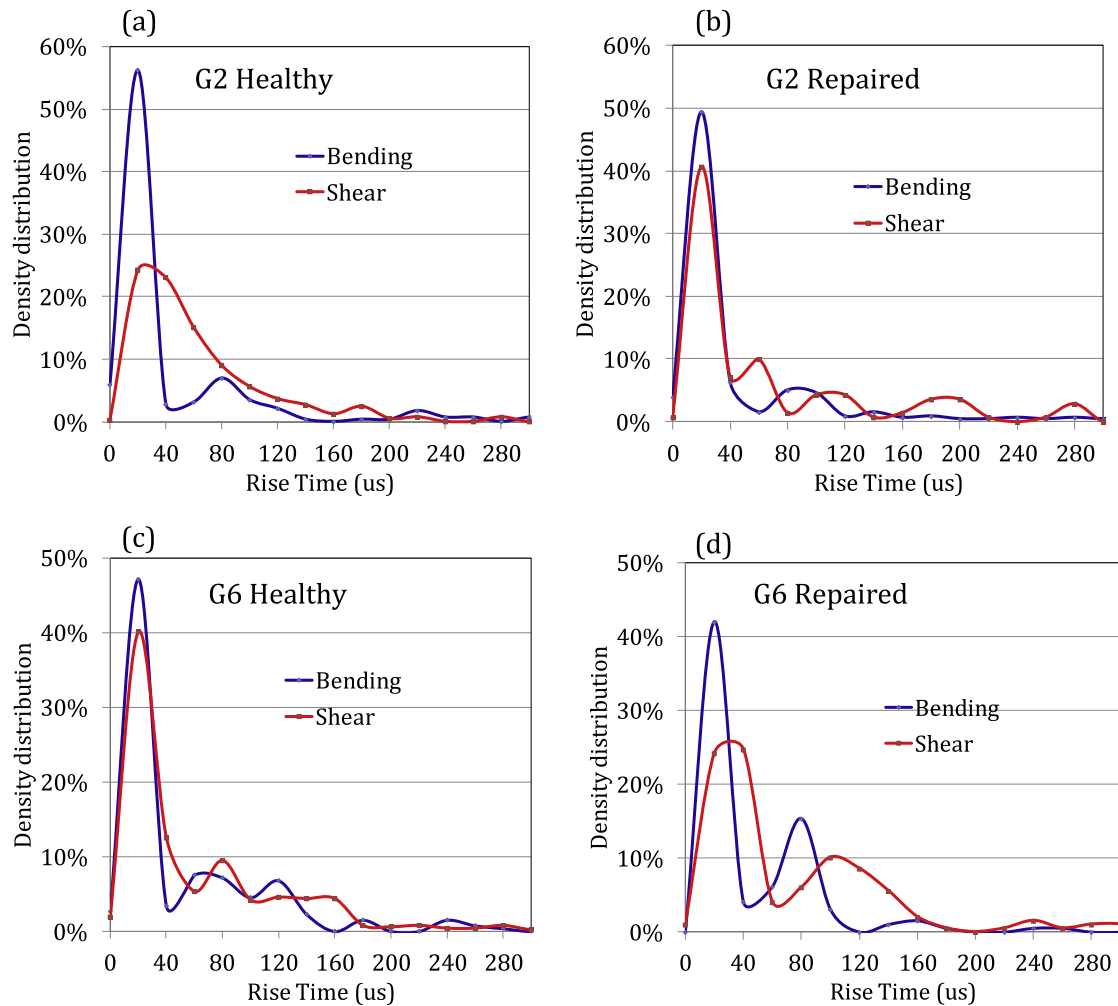


Fig. 10 – Density distributions of RT for AE populations at moderate load (class 1). (a) G2 Healthy, (b) G2 Repaired, (c) G6 Healthy, (d) G6 Repaired.



**Fig. 11 – Density distributions of RT for AE populations at high load (class 2). (a) G2 Healthy, (b) G2 Repaired, (c) G6 Healthy, (d) G6 Repaired.**

fracture starts, the process zone is affected “by the stress field generated by the fracture itself” [33] and simulations become much more difficult and would need more details to yield reliable results. Thus, it is argued that the stress field is dynamic and changes continuously after each crack propagation event compared to the initial static field. However, due to the different starting points of fracture (high normal stress in the one experiment and high shear in the other), there are still considerable changes in the fracture behavior as monitored by the AE parameters.

In the “shear” experiment, in order for the fracture to be developed in the specific intended way, the notches were necessary. After breaking some specimens it was made clear that notches were important to achieve the fracture in the predefined zone. Else, several specimens were fractured again near the middle, where the shear stresses are lower and normal are higher. By making the notches, the cross section is reduced in the targeted zone and the fracture zone is dictated to occur at the point where shear stresses are higher. Thus the comparison between the bending and “shear” test was possible. Additionally the notches were essential for the reliability of the AE measurements. In order to be able to

collectively study all experiments, the distance between the fracture zone and the sensors should be similar. Else if the location of crack was random, due to attenuation and distortion of the signal, a few additional cm would not allow studying the signals as one group. In order to check only the effect of fracture mode, it was necessary to fix the other parameters (like propagation distance between source and receiver) so that they do not crucially influence our result. The first sensor was in all cases 2 cm from the zone of the crack. The second was another 4 cm away. The reason that both sensors were at the same side, is that this gives the opportunity in the near future to check the AE parameters in terms of their additional propagation distance from one to the other receiver. Since all sources are from the same side of the sensors, this additional distance can be useful for characterizing how the AE parameters change by the additional propagation of 40 mm between the two receivers.

Concerning the difference in the cumulative AE behavior between shear and bending it is difficult to state a specific reason. Failure under the shear loading registers a nearly constant AE rate until failure without plateaus. The reason is difficult to conclude from this experimental study. This cannot

be related to literature since previous works do not target two distinct tests like herein, but a single test type (usually compressive) which leads to all different fracture events (tension, shear, mixed). In most of the cases these modes coexist [5,23,31,33]. This behavior seems to be a finding to be explored further.

## 5. Conclusions

The paper describes and discusses the fracture behavior of two granite types under different modes. Tests were accompanied by ultrasonic assessment before loading and acoustic emission monitoring during loading. The two granite types exhibited quite consistent behavior either in bending or shear exhibiting the similar trends in AE cumulative history and AE parameter values. This cannot be said for the adhesively repaired version of the specimens during the second loading as each specimen behaved in a unique way. Apart from the fact that ultrasonic pulse velocity is considerably higher for higher strength granite, the basic conclusions are mentioned below:

- i) The characteristics of AE waveforms are directly sensitive to the loading pattern (bending or shear). When preliminary damage is building up during moderate shear loading, AE signals have much longer RT than the corresponding bending damage. This direct correspondence between the initial stress field and the AE waveform parameters has not been explored in granite before. It allows to get information on the fracture very early in loading and before serious damage starts to be inflicted.
- ii) Shear loading produces a more continuous acoustic activity compared to bending. This implies that while bending damage resumes after periods of silent stress build-up, the shear goes on without serious “plateaus”.
- iii) Repair by means of epoxy in between the crack faces, restores the load bearing capacity up to 70% for bending and up to 40% for shear loading.
- iv) Repaired specimens exhibit longer initial silent periods in bending. This behavior is attributed to the elasticity of epoxy which allows straining longer before starting to have irreversible damage than granite itself.

This study shows that passive monitoring by AE can provide information on the stress field and the fracture pattern which cannot be provided by other non invasive techniques. The research continues with several other types of granite as well as marble materials. The effect of attenuation due to damping will be studied through the results of multiple sensors, something that will help to upgrade the test to larger geometries.

## Acknowledgements

The authors gratefully acknowledge Skandalis S.A. from Petralona Ioanninon, Greece for kindly supplying the specimens and Dipl. Eng. Th. Zampakolas for his contribution in conducting the fracture experiments.

This research project has been co-financed by the European Union (European Regional Development Fund–ERDF) and Greek national funds through the Operational Program “THESSALY, MAINLAND GREECE AND EPIRUS-2007-2013” of the National Strategic Reference Framework (NSRF 307 2007–2013).

## REFERENCES

- [1] M. Ohtsu, Recommendations of RILEM Technical Committee 212-ACD: acoustic emission and related NDE techniques for crack detection and damage evaluation in concrete: 3. Test method for classification of active cracks in concrete structures by acoustic emission, *Materials and Structures* 43 (9) (2010) 1187–1189.
- [2] C.U. Grosse, M. Ohtsu, *Acoustic Emission Testing*, Springer, Heidelberg, 2008.
- [3] S. Mindess, Acoustic emission methods, in: V.M. Malhotra, N. J. Carino (Eds.), *CRC Handbook of Nondestructive Testing of Concrete*, CRC, Boca Raton, FL, 2004.
- [4] R. Vidya Sagar, B.K. Raghu Prasad, R.K. Singh, Kaiser effect observation in reinforced concrete structures and its use for damage assessment, *Archives of Civil and Mechanical Engineering* 15 (2015) 548–557.
- [5] A. Carpinteri, M. Corrado, G. Lacidogna, Heterogeneous materials in compression: correlations between absorbed, released and acoustic emission energies, *Engineering Failure Analysis* 33 (2013) 236–250.
- [6] H. Elaqr, N. Godin, G. Peix, M. R'Mili, G. Fantozzi, Damage evolution analysis in mortar, during compressive loading using acoustic emission and X-ray tomography: effects of the sand/cement ratio, *Cement and Concrete Research* 37 (2007) 703–713.
- [7] D.A. Lockner, J.D. Byerlee, V. Kuksenko, A. Ponomarev, A. Sidorin, Quasi static fault growth and shear fracture energy in granite, *Nature* 350 (1991) 39–42.
- [8] B. Goszczyńska, G. Swit, W. Trampczyński, A. Krampikowska, J. Tworzewska, P. Tworzewski, Experimental validation of concrete crack identification and location with acoustic emission method, *Archives of Civil and Mechanical Engineering* 12 (2012) 23–28.
- [9] Y. Kawasaki, T. Wakuda, T. Kobayashi, M. Ohtsu, Corrosion mechanisms in reinforced concrete by acoustic emission, *Construction and Building Materials* 48 (2013) 1240–1247.
- [10] Detecting the activation of a self-healing mechanism in concrete by acoustic emission and digital image correlation, *The Scientific World Journal* (2013), <http://dx.doi.org/10.1155/2013/424560>, Article number 424560.
- [11] L. Chen, C.P. Wang, J.F. Liu, Y.M. Liu, J. Liu, R. Su, J. Wang, A damage-mechanism-based creep model considering temperature effect in granite, *Mechanics Research Communications* 56 (2014) 76–82.
- [12] E. Verstrynghe, L. Schueremans, D. Van Gemert, M. Wevers, Monitoring and predicting masonry's creep failure with the acoustic emission technique, *NDT&E International* 42 (2009) 518–523.
- [13] K. Ohno, M. Ohtsu, Crack classification in concrete based on acoustic emission, *Construction and Building Materials* 24 (12) (2010) 2339–2346.
- [14] D.G. Aggelis, S. Verbruggen, E. Tsangouri, T. Tysmans, D. Van Hemelrijck, Characterization of mechanical performance of concrete beams with external reinforcement by acoustic emission and digital image correlation, *Construction and Building Materials* 47 (2013) 1037–1045.
- [15] C. Grosse, H. Reinhardt, T. Dahm, Localization and classification of fracture types in concrete with quantitative

- acoustic emission measurement techniques, *NDT&E International* 30 (4) (1997) 223–230.
- [16] A.C. Mpalaskas, I. Vasilakos, T.E. Matikas, H.K. Chai, D.G. Aggelis, Monitoring of the fracture mechanisms induced by pull-out and compression in concrete, *Engineering Fracture Mechanics* 128 (2014) 219–230.
- [17] D.G. Aggelis, A.C. Mpalaskas, T.E. Matikas, Investigation of different fracture modes in cement-based materials by acoustic emission, *Cement and Concrete Research* 48 (2013) 1–8.
- [18] D.G. Aggelis, A.C. Mpalaskas, T.E. Matikas, Acoustic signature of different fracture modes in marble and cementitious materials under flexural load, *Mechanics Research Communications* 47 (2013) 39–43.
- [19] A. Moropoulou, K. Polikreti, V. Ruf, G. Deodatis, San Francisco Monastery, Quito, Ecuador: characterisation of building materials, damage assessment and conservation considerations, *Journal of Cultural Heritage* 4 (2003) 101–108.
- [20] L. Chen, J.F. Liu, C.P. Wang, J. Liu, R. Su, J. Wang, Characterization of damage evolution in granite under compressive stress condition and its effect on permeability, *International Journal of Rock Mechanics & Mining Sciences* 71 (2014) 340–349.
- [21] T. Ishida, Acoustic emission monitoring of hydraulic fracturing in laboratory and field, *Construction and Building Materials* 15 (2001) 283–295.
- [22] C. Cerrillo, A. Jiménez, M. Rufo, J. Paniagua, F.T. Pachón, New contributions to granite characterization by ultrasonic testing, *Ultrasonics* 54 (2014) 156–167.
- [23] D. Lockner, The role of acoustic emission in the study of rock fracture, *International Journal of Rock Mechanics and Mining Sciences & Geomechanics Abstracts* 30 (7) (1993) 883–899.
- [24] Neotex SA, “Technical data sheet,” <http://www.neotex.gr/frontoffice/portal.asp?cpage=NODE&cnode=122&clang=1> (accessed 2/2015).
- [25] A. Chmel, I. Shcherbakov, A comparative acoustic emission study of compression and impact fracture in granite, *International Journal of Rock Mechanics & Mining Sciences* 64 (2013) 56–59.
- [26] T. Shiotani, Y. Oshima, M. Goto, S. Momoki, Temporal and spatial evaluation of grout failure process with PC cable breakage by means of acoustic emission, *Construction and Building Materials* 48 (2013) 1286–1292.
- [27] S. Shahidan, R. Pulin, N. Muhamad Bunnori, K.M. Holford, Damage classification in reinforced concrete beam by acoustic emission signal analysis, *Construction and Building Materials* 45 (2013) 78–86.
- [28] T. Watanabe, S. Nishibata, C. Hashimoto, M. Ohtsu, Compressive failure in concrete of recycled aggregate by acoustic emission, *Construction and Building Materials* 21 (2007) 470–476.
- [29] <http://www.pacndt.com/index.aspx?go=products&focus=Software/noesis.htm>.
- [30] D. Polyzos, A. Papacharalampopoulos, T. Shiotani, D.G. Aggelis, Dependence of AE parameters on the propagation distance, *Journal of Acoustic Emission* 29 (2011) 57–67.
- [31] L. Jian-po, L. Yuan-hui, X. Shi-da, X. Shuai, J. Chang-yu, Cracking mechanisms in granite rocks subjected to uniaxial compression by moment tensor analysis of acoustic emission, *Theoretical and Applied Fracture Mechanics* 75 (2015) 151–159.
- [32] D.C. Jansen, S.P. Shah, Effect of length on compressive strain softening of concrete, *Journal of Engineering Mechanics* 123 (1997) 25–35.
- [33] D.E. Moore, D.A. Lockner, The role of microcracking in shear-fracture propagation in granite, *Journal of Structural Geology* 17 (1) (1995) 95–114.